



Mesoscopic study on instability characteristics of residual coal pillars–roof system based upon domino effect in pillar goaf

Zhiqiang Wang · Jingkai Li · Lu Lin · Binyu Liu · Ivan Ushakov

Received: 3 July 2023 / Accepted: 26 August 2023
© The Author(s) 2023

Abstract The stability of pillar goaf is affected by the composite structure composed of residual coal pillars and roof, it is necessary to study the instability characteristics of residual coal pillars–roof system. Double coal pillar–roof combined bodies were constructed based on single coal pillar–roof combined body to characterize coal pillars–roof system in this paper. Through particle flow code (PFC), the instability modes of single combined body and double combined bodies with different combinations under uniaxial compression were studied from a mesoscopic perspective. With that, the instability criterions of double combined bodies were analyzed theoretically. The results show that the damage of single combined body and double combined bodies both have domino–type characteristics. During the single combined body is compressed, coal is broken firstly and induces rock damage. Meanwhile, the rock damage

aggravates the destruction of coal in turn. Finally, the overall body loses bearing capacity based upon domino effect. During the double combined bodies with same mechanical properties are compressed, the component bodies bear the external load evenly and deform harmoniously. During the double bodies with different mechanical properties are compressed, the low-strength component body is destroyed and reaches its bearing limit firstly. Synchronously, the whole system reaches the bearing peak. Thereafter, the external load originally borne by low-strength body gradually transfers to high-strength body. The high-strength body also reaches the bearing limit over time, and the second bearing peak appears synchronously for the whole system. The instability of a single coal pillar is the initial cause of the instability of the whole coal pillars–roof system. The instability of any single component body can be regarded as the overall instability criterion for double bodies with same properties, while the instability of the single component body with high strength should be regarded as the instability criterion for double bodies with different properties.

Z. Wang · J. Li (✉) · L. Lin · B. Liu
School of Energy and Mining Engineering, China
University of Mining and Technology (Beijing),
Beijing 100083, China
e-mail: jingkai0801@163.com

Z. Wang · J. Li · L. Lin · B. Liu
China-Russia Dynamics Research Center, China
University of Mining and Technology (Beijing),
Beijing 100083, China

J. Li · I. Ushakov
National University of Science and Technology ‘MISIS’,
Moscow, Russia 119049

Article highlights

- Single coal pillar–roof combined body and double coal pillar–roof combined bodies were constructed to characterize single coal pillar–roof system and coal pillars–roof system in pillar goaf respectively.

- The source inducement and mode of chain instability for coal pillars–roof system in pillar goaf were deduced.
- The instability criterions of double coal pillar–roof combined bodies with different combinations were established theoretically.

Keywords Double combined bodies · Load transfer · Domino-type damage · Bearing characteristics · Instability criterion

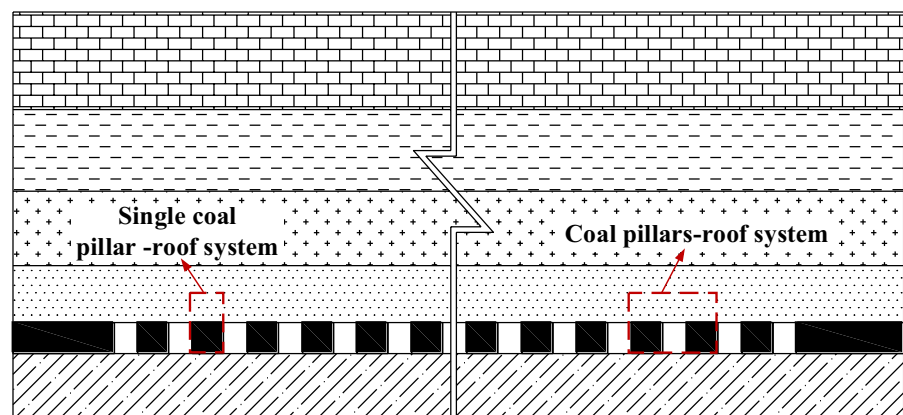
1 Introduction

After the underground coal seam is mined, a large-scale underground goaf will be formed. The stability of goaf is the key to ensure the safety of stope and surface (Liu et al. 2023; Pan et al. 2020). For ensuring the stability of underground goaf, a large number of coal pillars are set in and around the stope to support the overlying load (Han et al. 2022; Song et al. 2022). However, the residual coal pillars will be destroyed under plenty of factors over time (Zhu et al. 2019). To date, many researches have reflected that coal pillar is a part of coal–rock system (He et al. 2023). Further, the instability of coal pillar is caused by the combined action of coal and rock (Prasetyo et al. 2019). Therefore, it is of great significance to study the overall failure mode and mechanism of coal–rock system. Through numerical simulation and theoretical analysis, Zhou et al. (2021) showed that coal pillar is subjected to non-uniform load due to non-uniform deformation of roof, and the failure of coal pillar at different positions present different

characteristics. Qin et al. (2006) studied the failure mechanism of coal pillar–roof system through catastrophe theory and concluded that the instability of coal pillar mainly depends on the stiffness ratio of the whole system. Yin et al. (2021) compared the failure of coal–roof combined bodies with different rocks, it was found that the mechanical characteristics of combined bodies mainly depend on coal chiefly. Yang et al. (2015) theoretically analyzed the influence of roof structure on the bearing capacity and internal stress distribution in coal pillar. These results play an important guiding role for ensuring the stability of underground goaf.

However, as presented in Fig. 1, the residual coal pillars are set in the form of groups in pillar goaf. In this instance, the single coal pillar and its roof form single coal pillar–roof system, while coal pillars and roof form coal pillars–roof system. In the coal pillars–roof system, the interrelation and integration not only exist in among coal pillars, but also between coal pillars and roof (Li et al. 2020; Zhou et al. 2018). After a coal pillar becomes unstable, the overlying load it bore originally will transfer to the adjacent coal pillars, which may lead to the instability of adjacent coal pillars due to excessive load as well. By analogy, it is possible to trigger large-scale instability of coal pillars (Zhang et al. 2017). Thenceforth, the roof will break after reaching its ultimate bearing strength due to the loss of effective support from large-scale coal pillars. Meanwhile, the broken roof reacts to coal pillars and exacerbates their instability. Eventually, there will be a large area of instability in pillar goaf based upon the domino effect of coal pillars–roof system. However, the existing researches only consider the coal pillars as a whole to study its instability (Tian

Fig. 1 Engineering model of coal pillars–roof structure in pillar goaf



et al. 2023). Liu et al. (2021) demonstrated the gradual instability process of coal pillars and put forward that coal pillar reinforcement technologies can prevent the overall instability of goaf. Song et al. (2023) studied the failure characteristics of multiple coal pillars with different strengths, it was found that different coal pillars show imbalanced deformation characteristics. Feng et al. (2021) defined the “key pillars” in goaf and took it as the starting point to evaluate the instability of coal pillars.

In summary, there are few researches on instability of coal pillars–roof system that consider not only the interaction among coal pillars but also between coal pillars and roof based on domino effect. Therefore, the coal pillars–roof system is studied as a collaborative whole in this paper. The engineering model of coal pillars–roof system is difficult to be studied directly due to many factors (Bao et al. 2021; Zhukova et al. 2020). Thus, drawing on existing research methods, the coal–rock system in engineering was simplified as the coal–rock combined body (Li et al. 2022; Gao et al. 2020). The single coal pillar–roof combined body was designed firstly to characterize single coal pillar–roof system. Based on it, the double coal pillar–roof combined bodies with different combinations were also designed to characterize the coal pillars–roof system. The uniaxial compression tests were carried out by PFC. To point out the source inducement and load transfer characteristics of coal pillars –roof system, the damage process of single body and double bodies were recorded from the mesoscopic perspective. On this foundation, the instability criterions of double coal pillar–roof combined bodies with different combinations were established. The research results of this paper can provide theoretical and technical support for the prevention and control of domino—type disaster in pillar goaf.

2 Numerical model and procedure

2.1 Model setup

As a discontinuous medium programming software based on the discrete element method, PFC has significant advantages in simulating the mechanical behavior of coal and rock (Roos et al. 2019). In PFC program, the coal and rock models are composed of abundant tiny particles. By assigning geometric

parameters and mechanical parameters, models with identical mechanical properties or different mechanical properties can be established (Yin et al. 2019; Chen et al. 2020). The damage of coal and rock are realized by particle movement and interaction between particles, which can reflect the mechanical behavior of coal and rock more comprehensively from the mesoscopic perspective. Therefore, this study used PFC to simulate uniaxial compression of coal and rock. As coal and rock are aggregates composed of mineral particles, the contact between particles mostly adopts parallel bonding model in the PFC model. The parallel bonding model can transmit force and moment at the same time, which is more realistic (Poulsen et al. 2018).

Under the same roof in pillar goaf, the mechanical properties of coal pillars may be the same or similar, or there may be obvious differences. Therefore, to construct combined bodies with different combinations, two types of coal with different mechanical properties were selected, and the same sandstone was selected for the rock. As presented in Fig. 2a, b, single coal pillar–roof body A (SCRA) and single coal pillar–roof body B (SCRB) were designed. Factors such as height and interface were not considered (Liu et al. 2018; Yu et al. 2022; Sun et al. 2021). The overall sizes of models are 50 mm×100 mm, the height ratio of coal and rock is 1:1, the lower part is coal and the upper is rock. Furthermore, two series of double coal pillar–roof bodies composed of two single bodies with the same mechanical properties were designed, which are named double coal pillar–roof bodies A (DCRAA) and double coal pillar–roof bodies B (DCRBB) respectively, as presented in Fig. 2c, d. Meanwhile, double bodies composed of two single bodies with different mechanical properties were designed as well, which is named double coal pillar–roof bodies AB (DCRAB), as presented in Fig. 2e. To avoid the influence of geometric parameters on the results, the geometric parameters in all models are kept consistent. When modeling, a single coal pillar–roof model was established and preserved after preloading firstly. In subsequent simulations, the corresponding mechanical parameters were given after calling this model. For the modeling of double coal pillar–roof bodies, the saved single coal pillar–roof model was first called to generate one side of the double bodies, and then

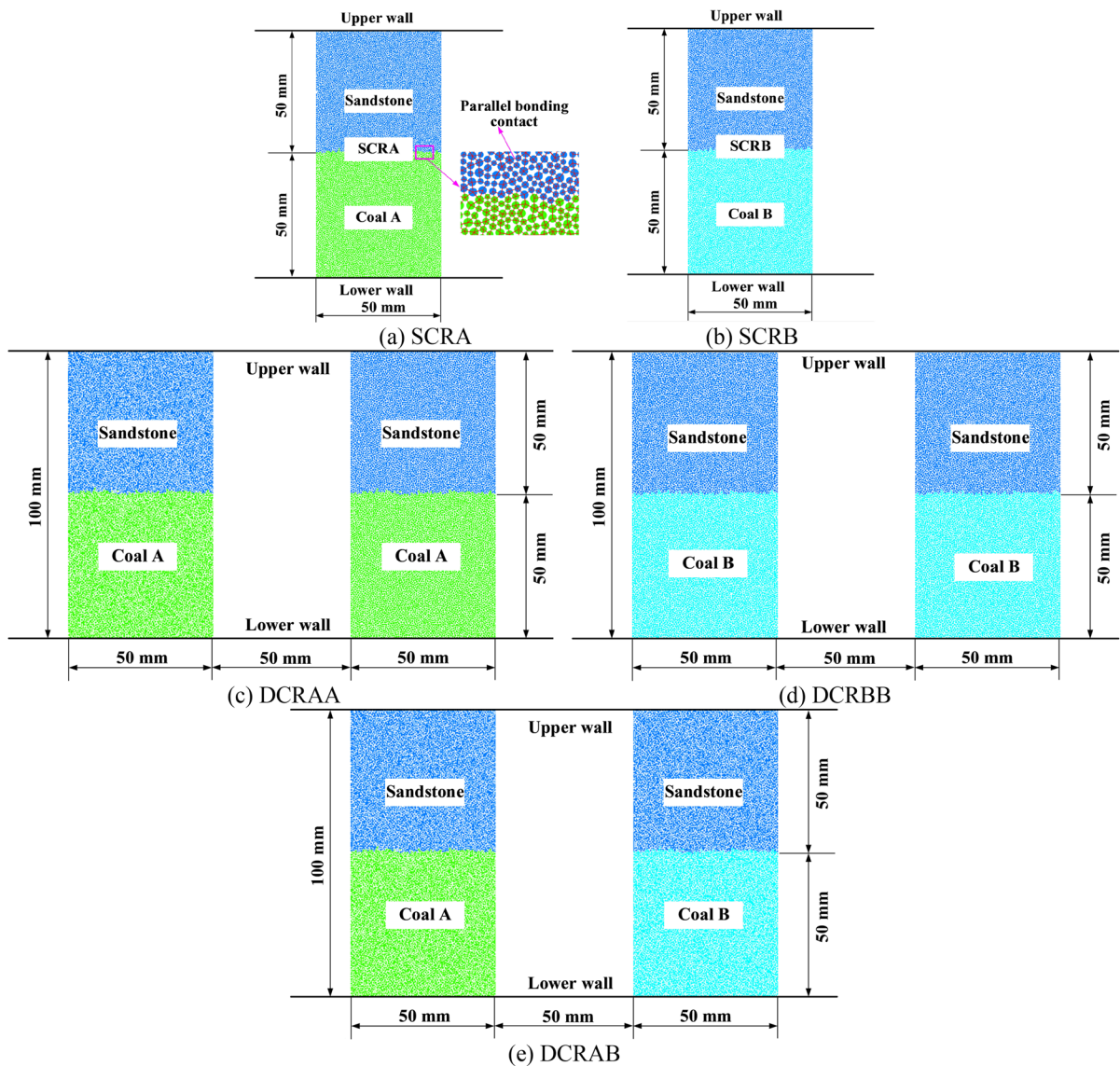


Fig. 2 Numerical model

it was copied and moved by FISH language to get the other side of double bodies. Moreover, based on the existing experimental design methods of coal pillars in coal mines and pillars in non-coal mines (Bai 2019; Zhou et al. 2020), the influence of distances among coal pillars were also not considered during the establishment of the double bodies, but the distance between the two component bodies remains consistent all the time.

2.2 Mesoscopic parameters confirmation

To make the PFC model consistent with the macroscopic mechanical properties of actual coal and rock, the "trial-and-error method" was applied to calibrate the mesoscopic parameters in combination with laboratory tests, which was carried out before uniaxial compression simulation of combined bodies. When the stress–strain curve and failure mode of the PFC

simulation are in good agreement with that of the laboratory test, it is considered that the microscopic parameters meet the simulation requirements (Sarfazai et al. 2023; Ozturk et al. 2017). The PFC model of each coal or rock was set as a two-dimensional rectangle of 50 mm×100 mm, and the corresponding laboratory prototype is a standard specimen of φ 50×100 mm. Displacement loading method was applied in both laboratory test and numerical simulation, the loading rates were both 0.05 mm/s.

The comparisons of laboratory tests and numerical simulations for each specimen are presented in Fig. 3. The experimental peak strengths of coal A, coal B and sandstone are 19.21 MPa, 10.02 MPa and 39.35 MPa respectively, while the numerical peak strengths are 19.44 MPa, 10.14 MPa and 39.89 MPa respectively. The experimental peak strength strains

of coal A, coal B and sandstone are 0.74%, 0.87% and 1.17% respectively, while the numerical peak strength strains are 0.71%, 0.84% and 1.14% respectively. There is a difference between the numerical simulations and laboratory tests, especially the difference in strains. That is because the numerical models are composed of uniformly distributed rigid particles with the same mechanical parameters, while the mechanical parameters of the mineral particles that make up the laboratory bodies are discrete. Additionally, there are many randomly distributed original pores and cracks in the laboratory bodies (Chen et al. 2023). Therefore, the experimental and numerical stress–strain curves cannot completely coincide, especially the numerical stress–strain curve does not have the stage of original pore compaction, but the experimental stress–strain curve does, which leads to the

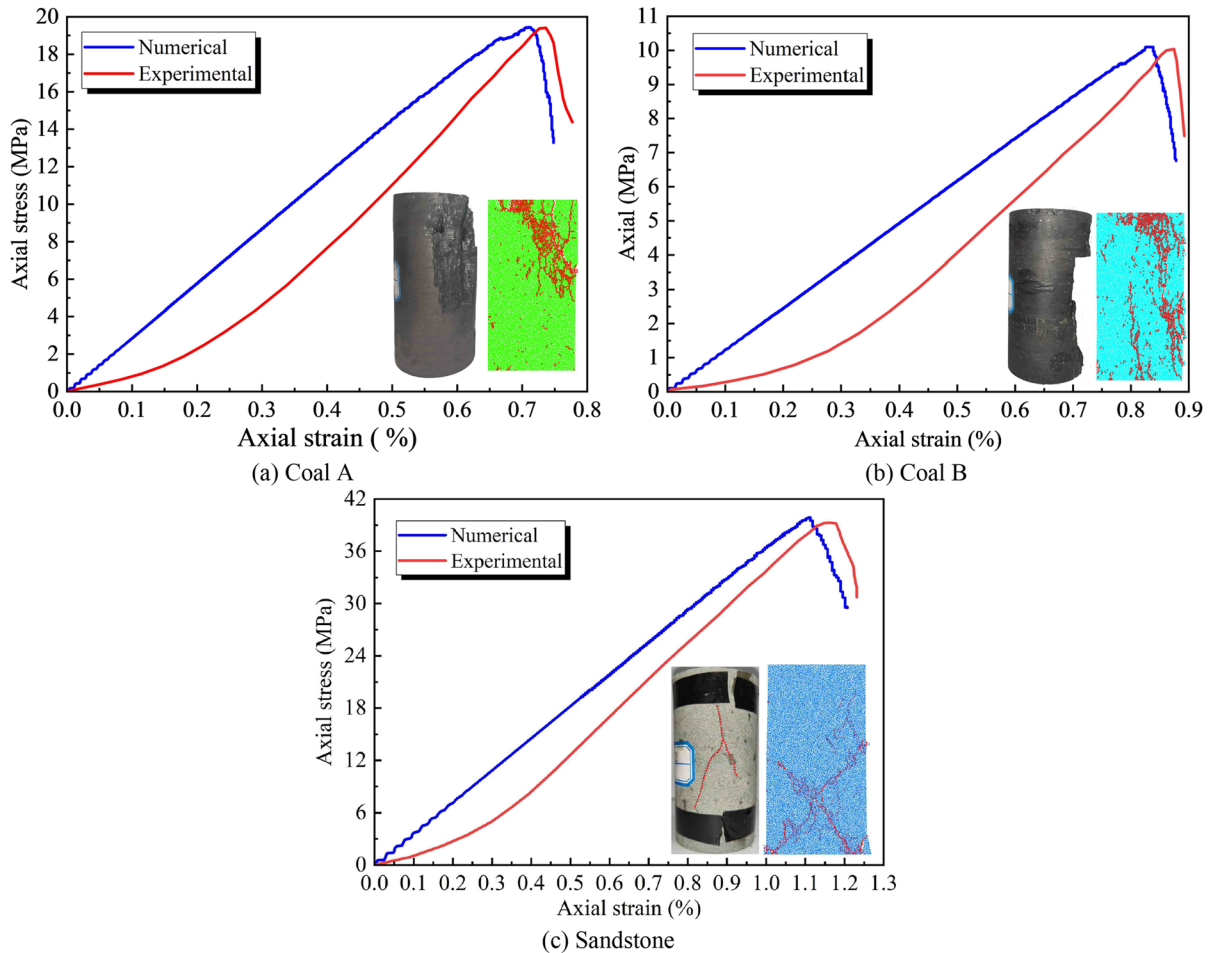


Fig. 3 Comparisons between numerical simulations and laboratory tests

Table 1 Some basic mesoscopic parameters

Meso-parameters	Sandstone	Coal A	Coal B
Particle density/(kg m ⁻³)	2850	1800	1300
Radius/mm	0.28–0.46	0.28–0.46	0.28–0.46
Frictional coefficient	0.7	0.5	0.4
Contact modulus/GPa	20.2	3.5	2.4
Parallel bonding modulus/GPa	20.2	3.5	2.4
Tangential bonding strength/MPa	38	24	12
Normal bonding strength/MPa	36	14	8

numerical strain is greater than the experimental one. However, for all that, the stress–strain curves and the final failure models of laboratory tests and numerical simulations are close to each other relatively. To sum up, the calibrated mesoscopic parameters can be applied to simulate the mechanical behavior of experimental coal and rock. Some specific mesoscopic parameters are presented in Table 1.

2.3 Simulation procedure

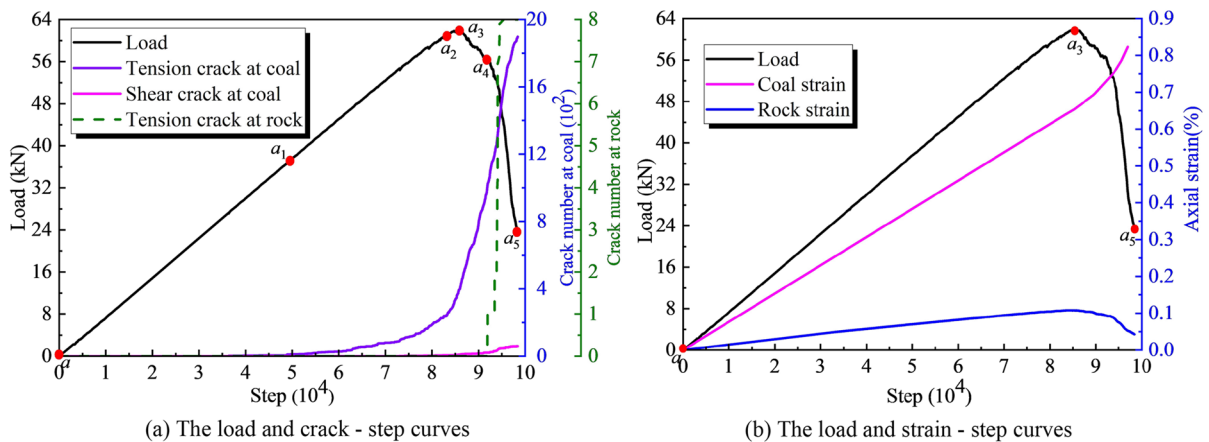
The uniaxial compression simulation of each single combined body and double combined bodies were carried out in sequence. Uniaxial compression was realized by displacement loading, that is, vertical downward displacement was applied to the upper wall. Meanwhile, vertical upward displacement was

applied to the lower wall. The loading rate was fixed at 0.05 mm/s all the time. The uniaxial compression was stopped when the model was destroyed (Zhao et al. 2021). During the compression of single combined body, the load was obtained by monitoring the counterforce of boundary walls. For the double coal pillar–roof combined bodies, the stress of each component body was monitored separately during the compression, and the load was obtained by multiplying the stress by the cross-sectional area. Similarly, the total load borne by the double combined bodies was also obtained by monitoring the counterforce of the boundary walls. Meanwhile, FISH language was adopted to monitor the average strain of each body in real time.

3 Results analysis

3.1 Single combined body

The bearing and deformation laws of SCRA and SCRB are presented in Figs. 4 and 5 respectively. Different characteristic points were selected on the load–step curves to analyze the failure process, as presented in Table 2 and Table 3 respectively. Explanatorily, the black symbols in the bodies indicate tension cracks and the red symbols indicate shear cracks. Although the loads of the two types of bodies are different, the failure modes are the same. The bodies

**Fig. 4** Bearing capacity and deformation laws of SCRA

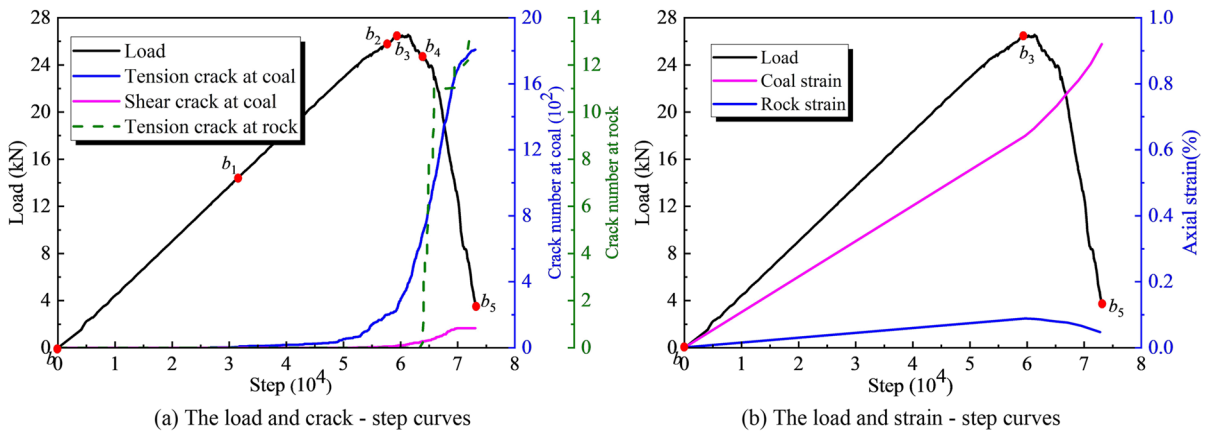


Fig. 5 Bearing capacity and deformation laws of SCRB

Table 2 Failure process of SCRA

Position	<i>a</i>	<i>a</i> ₁	<i>a</i> ₂	<i>a</i> ₃	<i>a</i> ₄	<i>a</i> ₅
Model						

Table 3 Failure process of SCRB

Position	<i>b</i>	<i>b</i> ₁	<i>b</i> ₂	<i>b</i> ₃	<i>b</i> ₄	<i>b</i> ₅
Model						

both go through the process of “cracks initiation-cracks propagation-cracks penetration”, which finally leads to the macroscopic failure. According to the laws of cracks development in different locations and types, the failure can be subdivided into five stages.

Stage I (a–a₁, b–b₁): Stage of coal tension cracks initiation. At the initial stage of axial compression,

external load cannot break the bonds among model particles yet. Subsequently, the increase of interparticle force induces tension stress concentration at coal with loading. The bonds among the particles at the stress concentration exhibit tension fractures, leading to the initiation of tension cracks at the coal.

Stage II (a_1 – a_2 , b_1 – b_2): Stage of coal shear cracks initiation. The tension cracks propagate slowly and penetrate partially. At the same time, shear cracks initiate due to the shear fractures of bonds among particles at coal.

Stage III (a_2 – a_3 , b_2 – b_3): Stage of slow coal cracks propagation and penetration. The number and penetration of coal cracks continued to increase before the peak load, but the increase rate is still slow.

Stage IV (a_3 – a_4 , b_3 – b_4): Stage of rock tension cracks initiation. After the peak load, the number and penetration of coal cracks increase significantly at a high rate, and the rock tension cracks initiate near the interface of coal and rock as well. Meanwhile, the bearing capacity of whole body decreases gradually.

Stage V (a_4 – a_5 , b_4 – b_5): Stage of rapid cracks penetration. Although rock cracks continue to increase and propagate, the overall number is small relatively, while the speed and degree of coal failure increase significantly, especially the shear cracks. Microcracks propagate and penetrate to form a “V” shaped macroscopic crack at coal, leading to the overall instability of combined body ultimately.

As presented in Figs. 4b and 5b, the strains of coal and rock present different evolutions. Meanwhile, the strain of coal is far greater than that of rock. The strain of coal increases continuously, and the rate increases obviously after the peak load, while the strain evolution of rock is consistent with the load. That is, the strain of rock increases linearly

before the peak load, but decreases parabolically at a relatively small rate after the peak load.

Generally speaking, coal dominates the destruction of single combined body. The coal is broken firstly and induces rock damage and the rock damage aggravates the destruction of coal in turn. Finally, the overall body loses bearing capacity based upon domino effect. It is inferred that there is domino-type instability in the “small system” composed of single coal pillar and its roof. If a single coal pillar is destroyed, it will lead to the deformation of the roof easily. Afterwards, the roof deformation will aggravate the destruction of coal pillar, which lead to the overall instability of single coal pillar–roof system.

3.2 Double combined bodies with same properties

The bearing and deformation laws of DCRAA and DCRBB are presented in Figs. 6 and 7. Similarly, different characteristic points were selected on the load–step curves to analyze the failure characteristics. The failure processes of double bodies are presented in Tables 4 and 5. Explanatorily, taking DCRAA as an example, “LCRA” represents the left component body and “RCRA” represents the right one; “LCA” represents the left coal and “RCA” represents the right one; “LR” represents the left rock and “RCA” represents the right one. The same representation is applied in subsequent simulation.

Although the loads are different, the bearing and failure characteristics of the two series are similar. In each series, the load–step curves of two component

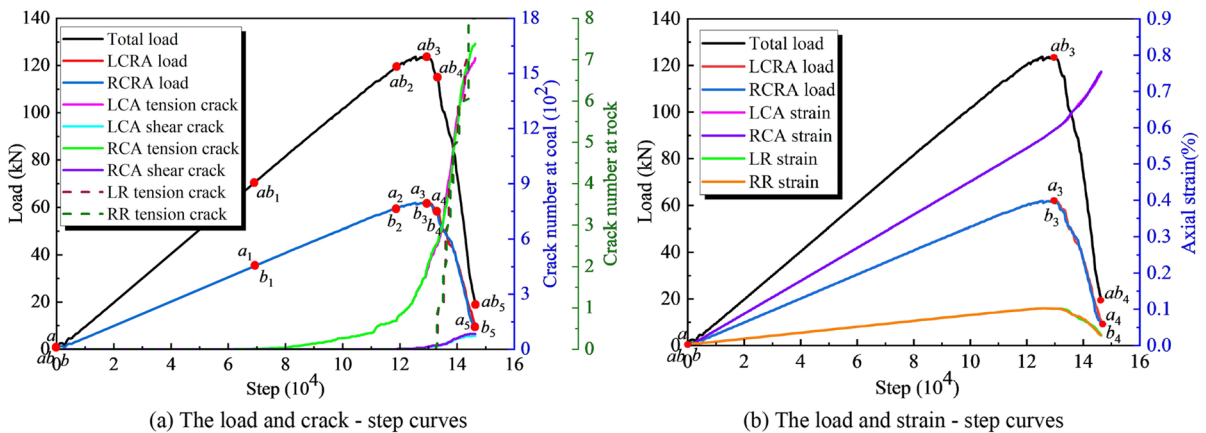


Fig. 6 Bearing capacity and deformation laws of DCRAA

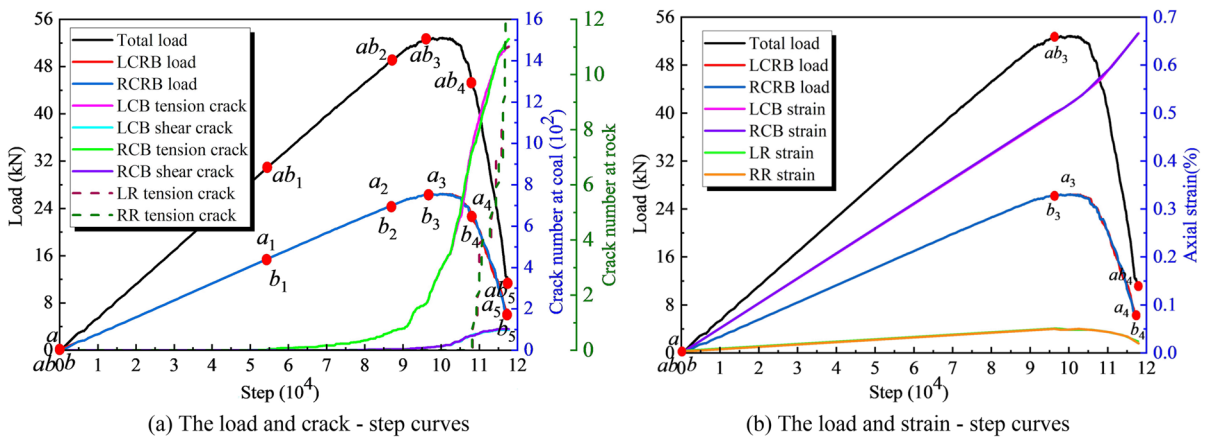


Fig. 7 Bearing capacity and deformation laws of DCRBB

Table 4 Failure process of DCRAA

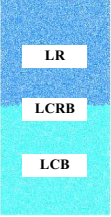
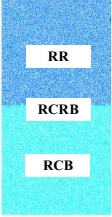
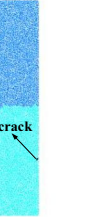
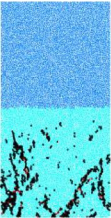
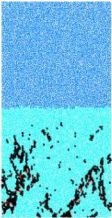
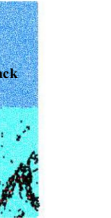
Position	a, b, ab	a_1, b_1, ab_1	a_2, b_2, ab_2
Model			
Position	a_3, b_3, ab_3	a_4, b_4, ab_4	a_5, b_5, ab_5
Model			

bodies are highly coincident with each other. Concomitantly, two component bodies divide the external load uniformly during uniaxial compression. Meanwhile, the peak loads of two component bodies are equal basically. Synchronously, not only the strain laws of component bodies are consistent, but also the cracks initiation, propagation and penetration occur simultaneously with the highly consistent number and mode. In addition, the evolution law of the total load–step curve of the whole system is consistent with that of any component body, but the total load is much greater than either of them. With the

synchronous failure of the two component bodies, the whole system loses its bearing capacity immediately as well.

To sum up, the bearing and deformation characteristics of double bodies with same mechanical properties are similar to those of single combined bodies mentioned above. According to the development of different positions and types about cracks, the failure of the whole double bodies system can be also subdivided into the five stages mentioned above. Likewise, the damage of component bodies still occurs in coal mainly, while only a few cracks in rock appear

Table 5 Failure process of DCRBB

Position	a, b, ab	a_1, b_1, ab_1	a_2, b_2, ab_2
Model			
Position	a_3, b_3, ab_3	a_4, b_4, ab_4	a_5, b_5, ab_5
Model			

near the interface. However, different from the single body mentioned above, the double bodies with the same mechanical properties not only have domino—type damage in the “small system” for each component body, but also has domino—type damage in the whole “big system” composed of component bodies. Specifically, the mechanical properties of the left and right bodies are the same, if any one of them is destroyed, the other body will destroy synchronously due to the domino effect, which will lead to the rapid

instability of the whole double bodies system. It can be inferred that under the same roof condition in pillar goaf, for coal pillars with the same or similar mechanical properties, all the coal pillars are distributed evenly and deformed synchronously. If a coal pillar is damaged and unstable, it will cause large-scale coal pillars instantly. After that, wide roof may collapse synchronously without support, resulting in goaf disaster finally.

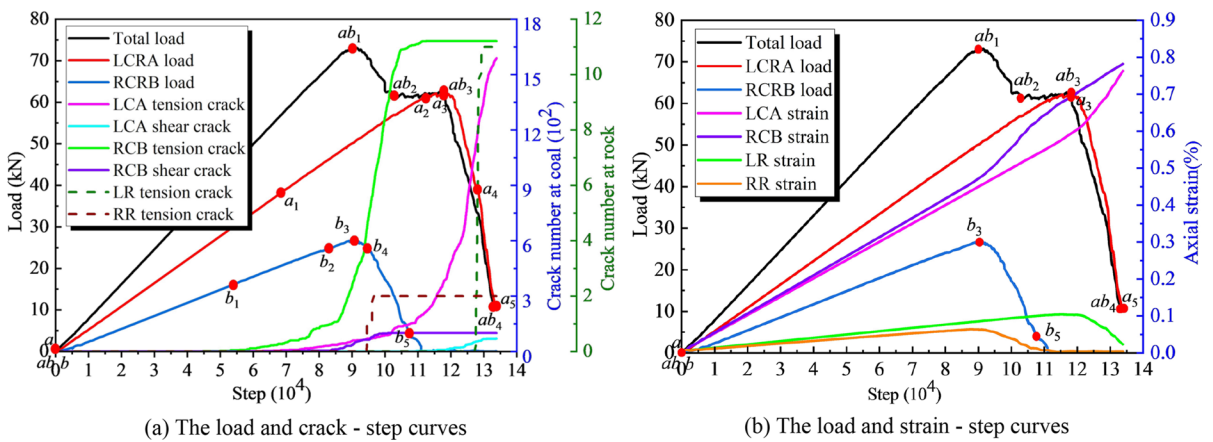


Fig. 8 Bearing capacity and deformation laws of DCRAB

Table 6 Failure process of DCRAB

Position	a, b, ab			b_1		a_1	
Model							
Position	b_2		ab_1, b_3		b_4		
Model							
Position	ab_2		b_5		a_2		
Model							
Position	a_3, ab_3		a_4		a_5, ab_4		
Model							

3.3 Double combined bodies with different properties

Uniaxial compression simulation was carried out on the double coal pillar–roof bodies composed of single body A and single body B with different mechanical properties. Figure 8 presents the bearing capacity and deformation laws of DCRAB, and Table 6 presents the failure process. The load–step curve of any component body in DCRAB shows the same evolution as that of the single body and the double bodies with same properties mentioned above, but the total

load–step curve shows obvious differences with them. According to the law of total load–step curve, the instability of DCRAB can be divided into four stages.

Stage I (ab–ab₁): Stage of load linear increase. At the initial stage of loading, the total load and the load of each component body increase linearly. Meanwhile, the strain of each coal and rock increases linearly as well. At the same time, combined with Table 6, it can be seen that RCB first initiates tension and shear microcracks in turn. With loading, these microcracks propagate, pen-

etrate and form macrocracks eventually, while only a few tension microcracks distributed randomly and appear at RCA evenly. As the load of RCRB reaches its peak, the total load also reaches the peak synchronously.

Stage II (ab_1 – ab_2): Stage of gradually weakening load. After the peak load of RCRB, its bearing capacity begins to decrease, while the bearing capacity of LCRA is still in the stage of linear increase. The decrease in bearing capacity of RCRB is greater than the increase of LRCA, so the total load decreases slowly. The strain rate of RCB increases with its failure, and the RR strain rebounds after reaching its peak. Additionally, tension microcracks appear at RR near the interface. On the contrary, the strains of LCA and LR still increase linearly, and the tension microcracks at LCA are still distributed randomly and evenly with few numbers.

Stage III (ab_2 – ab_3): Stage of secondary load increase. The load of LCRA still increases and reaches the peak gradually, while RCRB gradually loses its bearing capacity completely. During this period, the load RCRB borne originally transfers to LCRA slowly, which leads to LCRA gradually becoming the main bearing body. Because the increase in bearing capacity of LRCA is greater than the decrease of RCRB, although the total load evolution oscillates slightly, it shows an overall increasing trend. Concomitantly, the second total load peak appears when LCRA reaches its peak load. Additionally, the strains of LCA and LR still increase linearly. The tension microcracks in LCA continue to develop and macrocracks begin to form locally.

Stage IV (ab_3 – ab_4): Stage of rapid load decline. After the peak load of LCRA, the rapid increase of cracks leads to the destruction of LCA. Meanwhile, tension microcracks also appear at LR. Subsequently, the failure of LCRA leads to the rapid decline of the total load. Finally, the whole system of DCRA loses bearing capacity synchronously with the instability of LCRA.

From the above analysis, it can be seen that double bodies with different mechanical properties also have domino—type instability in the whole "big system" during uniaxial compression. Specifically, after the component body with low strength becomes

instability firstly, the external load originally borne by it transfers to another component body with high strength. The component body with high strength is destroyed due to the increase of external load, which leads to instability of the whole system eventually. Therefore, it is considered that if the mechanical properties of coal pillars are different under the same roof in pillar goaf, the single coal pillar with the weakest bearing capacity loses stability firstly, which leads to load transfer and domino—type failure of other coal pillars. After losing the effective support of the coal pillars in a large area, the roof will collapse in a wide range.

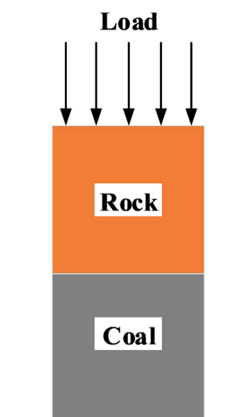
Overall, whether it is for double combined bodies with same properties or different properties, the overall failure of the whole system is caused by the instability of one of the component bodies. Meanwhile, the instability of the component body is caused and dominated by the destruction of coal. Therefore, the instability of a single coal pillar is the initial cause of the instability of the whole coal pillars–roof system. That is, the instability of a single coal pillar is equivalent to triggering the first card in the "Domino" of coal pillars–roof system, which leads to chain disasters in the "big system" composed of coal pillars and roof easily.

4 Establishment of instability criterion

4.1 Single combined body bearing capacity

As presented in Fig. 9, the uniaxial loading model of the single combined body is established without considering the influence of the interface between coal

Fig. 9 Schematic diagram of the single body under uniaxial loading



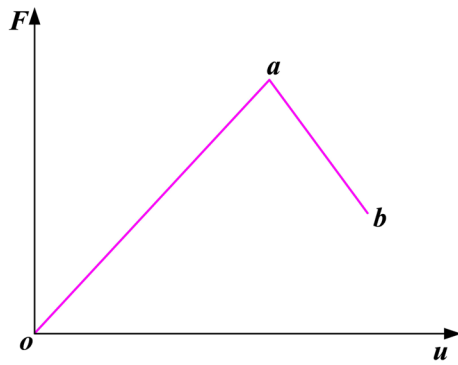


Fig. 10 Elastic-strain softening constitutive relationship

and rock (Huang et al. 2013; Liu et al. 2015). The coal and rock of the combined body both meet the elastic-strain softening constitutive equation, as presented in Fig. 10 (Yang 2019).

During the early stage of compression, both the coal and rock of the combined body are in the elastic stage, which is the section *oa* in Fig. 10. During this stage, both the coal and rock meet the following requirement:

$$\sigma = E\varepsilon \tag{1}$$

where σ represents the axial stress; E represents the elastic modulus of coal or rock; ε represents the strain of coal or rock.

As the force is transmitted equally in the combined body, it can be seen that:

$$E_c \varepsilon_c S_c = E_r \varepsilon_r S_r \tag{2}$$

where E_c represents the elastic modulus of coal; ε_c represents the strain of coal; S_c represents the cross-sectional area of coal; E_r represents the elastic modulus of rock; ε_r represents the strain of rock; S_r represents the cross-sectional area of rock.

The total axial deformation of the combined body is:

$$\varepsilon_c h_c + \varepsilon_r h_r = u \tag{3}$$

where h_c represents the height of coal; h_r represents the height of rock; u represents the total axial deformation of the single combined body.

By combining Eqs. (2) and (3), it can be concluded that:

$$\varepsilon_c = \frac{E_r S_r}{E_r S_r h_c + E_c S_c h_r} u \tag{4}$$

The overall bearing capacity of the combined body in the elastic stage can be expressed as:

$$F_1 = \frac{E_c E_r S_r S_c}{E_r S_r h_c + E_c S_c h_r} u \tag{5}$$

With the compression, the coal in the combined body reaches the peak bearing capacity firstly. At the same time, the whole body reaches the peak bearing capacity as well. And then the coal enters the strain softening stage, which is the section *ab* in Fig. 10, while the rock is still in the elastic stage.

After coal enters the strain softening stage, it meets the following requirement:

$$\sigma' = \sigma_a - E'_c (\varepsilon_c - \varepsilon_{ca}) \tag{6}$$

where σ' represents the axial stress of coal in the descending section of *ab*; σ_a represents the peak strength of coal; E'_c represents the slope of coal in the descending section of *ab*; ε_{ca} represents the peak strength strain of coal.

By equally transmitting force within the combined body, it can be concluded that:

$$[\sigma_a - E'_c (\varepsilon_c - \varepsilon_{ca})] S_c = E_r \varepsilon_r S_r \tag{7}$$

By combining Eqs. (3) and (7) and substituting $\varepsilon_{ca} = \sigma_a / E'_c$ into them, it can be concluded that:

$$\varepsilon_r = \frac{1}{E_c} \frac{E_c S_c \sigma_a h_c + E'_c S_c \sigma_a h_c - E_c S_c E'_c u}{E_r S_r h_c - E'_c S_c h_r} \tag{8}$$

The overall bearing capacity of the combined body can be represented as:

$$F_2 = \frac{E_r S_r}{E_c} \left(\frac{E_c S_c \sigma_a h_c + E'_c S_c \sigma_a h_c}{E_r S_r h_c - E'_c S_c h_r} - \frac{E_c S_c E'_c}{E_r S_r h_c - E'_c S_c h_r} u \right) \tag{9}$$

In summary, the expression for the bearing capacity of the single combined body is:

$$F = \begin{cases} \frac{E_c E_r S_r S_c}{E_r S_r h_c + E_c S_c h_r} u, & 0 < u_c \leq u_{ca} \\ \frac{E_r S_r}{E_c} \left(\frac{E_c S_c \sigma_a h_c + E'_c S_c \sigma_a h_c}{E_r S_r h_c - E'_c S_c h_r} - \frac{E_c S_c E'_c}{E_r S_r h_c - E'_c S_c h_r} u \right), & u_{ca} < u'_c < \infty \end{cases} \tag{10}$$

where u_c represents the displacement of coal in section oa ; u_{ca} represents the displacement of coal at the peak bearing capacity; u_c' represents the displacement of coal in section ab .

4.2 Instability criterion of double bodies with same mechanical properties

Combined with the numerical simulation results, the load–displacement curves of double bodies with the same mechanical properties are presented in Fig. 11, which is consistent with the load–displacement curve of single body under load. The whole system is unstable synchronously after any component body loses its stability, so the instability criterion of any component body can be used as the instability criterion of the whole system. This paper takes the left component body as an example to analyze.

The overall bearing capacity of the double bodies with same mechanical properties can be expressed as:

$$F_s = \begin{cases} 2 \frac{E_{cl}E_{rl}S_{rl}S_{cl}}{E_{rl}S_{rl}h_{cl} + E_{cl}S_{cl}h_{rl}} u_l, & 0 < u_{cl} \leq u_{cal} \\ 2 \frac{E_{rl}S_{rl}}{E_{cl}} \left(\frac{E_{cl}S_{cl}\sigma_{al}h_{cl} + E'_{cl}S_{cl}\sigma_{al}h_{cl}}{E_rS_rh_c - E'_cS_c h_r} - \frac{E_{cl}S_{cl}E'_{cl}}{E_{rl}S_{rl}h_{cl} - E'_{cl}S_{cl}h_{rl}} u_l \right), & u_{cal} < u'_{cl} < \infty \end{cases} \quad (11)$$

where F_s represents the total load of double bodies with same mechanical properties; the other parameters are all marked with a subscript l added to the corresponding parameters mentioned above, these parameters represent the same meaning, but the subscript l represents the left component body.

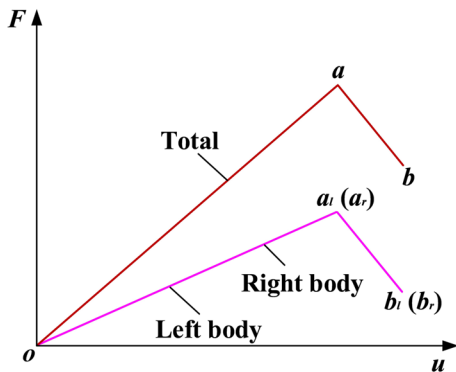


Fig. 11 Load–displacement curves of double combined bodies with same mechanical properties

The section oa in Fig. 11 corresponds to the first expression in Eq. (11). During this stage, the component bodies and the whole system are all in the elastic stage. Therefore, the whole system is stable. Section ab corresponds to the second expression in Eq. (11). During this stage, the bearing capacities of the component bodies and the whole system all begin to decline.

For the second expression in Eq. (11), if:

$$E_{rl}S_{rl}h_{cl} - E'_{cl}S_{cl}h_{rl} > 0 \quad (12)$$

Then the coefficient of displacement u_l is negative, indicating that the body still moves downward (when the displacement is vertically downward, it is in the negative direction). Although the bearing capacity of the body gradually decreases, the energy generated by external load can still be accumulated in the body, and the system still has bearing capacity at this time.

If:

$$E_{rl}S_{rl}h_{cl} - E'_{cl}S_{cl}h_{rl} < 0 \quad (13)$$

Then the coefficient of displacement u_l is positive, it means that the body moves upward. In this way, the body is broken seriously, which leads to the energy accumulated in it release and act externally. At this time, the body is unstable and no longer has the bearing capacity.

If:

$$E_{rl}S_{rl}h_{cl} - E'_{cl}S_{cl}h_{rl} = 0 \quad (14)$$

Then the coefficient of displacement u_l is negative infinity, the bearing capacity of the body is infinitely close to zero, which indicates that the body is in a critical instability state at this time and will be unstable once it is disturbed slightly.

To sum up, the stable state of the double bodies with same mechanical properties can be determined by Eqs. (12–14), which are the criterion for determining whether the double bodies with same

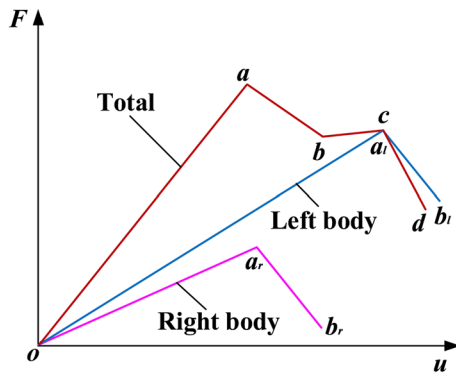


Fig. 12 Load–displacement curves of double combined bodies with different mechanical properties

mechanical properties are unstable. At the same time, it is specially explained that these three Equations are applicable to any left or right component body, the applicable conditions and results are consistent.

4.3 Instability criterion of double bodies with different mechanical properties

The load–displacement curves of the double bodies with different mechanical properties are presented in Fig. 12. The load–displacement curves of the left and right bodies are consistent with that of the single body, but the total load–displacement curve is different.

The overall bearing capacity of double bodies with different mechanical properties can be expressed by the following equation:

$$F_d = \begin{cases} \frac{E_{cl}E_{rl}S_{rl}S_{cl}}{E_{rl}S_{rl}h_{cl}+E_{cl}S_{cl}h_{rl}}u_l + \frac{E_{cr}E_{rr}S_{rr}S_{cr}}{E_{rr}S_{rr}h_{cr}+E_{cr}S_{cr}h_{rr}}u_r, & 0 < u_{cr} \leq u_{car} \\ \frac{E_{cl}E_{rl}S_{rl}S_{cl}}{E_{rl}S_{rl}h_{cl}+E_{cl}S_{cl}h_{rl}}u_l + \frac{E_{rr}S_{rr}}{E_{cr}} \left(\frac{E_{cr}S_{cr}\sigma_{ar}h_{cr}+E'_{cr}S_{cr}\sigma_{ar}h_{cr}}{E_{rr}S_{rr}h_{cr}-E'_{cr}S_{cr}h_{rr}} - \frac{E_{cr}S_{cr}E'_{cr}}{E_{rr}S_{rr}h_{cr}-E'_{cr}S_{cr}h_{rr}}u_r \right), & u_{car} < u_{cl} \leq u_{cal} \\ \frac{E_{rl}S_{rl}}{E_{cl}} \left(\frac{E_{cl}S_{cl}\sigma_{al}h_{cl}+E'_{cl}S_{cl}\sigma_{al}h_{cl}}{E_{rl}S_{rl}h_{cl}-E'_{cl}S_{cl}h_{rl}} - \frac{E_{cl}S_{cl}E'_{cl}}{E_{rl}S_{rl}h_{cl}-E'_{cl}S_{cl}h_{rl}}u_l \right) + \frac{E_{rr}S_{rr}}{E_{cr}} \left(\frac{E_{cr}S_{cr}\sigma_{ar}h_{cr}+E'_{cr}S_{cr}\sigma_{ar}h_{cr}}{E_{rr}S_{rr}h_{cr}-E'_{cr}S_{cr}h_{rr}} - \frac{E_{cr}S_{cr}E'_{cr}}{E_{rr}S_{rr}h_{cr}-E'_{cr}S_{cr}h_{rr}}u_r \right), & u_{cal} < u'_{cl} < \infty \end{cases} \quad (15)$$

where F_d is the total load of double bodies with different mechanical properties; the subscript l and r represent the left and right component body respectively.

The section oa in Fig. 12 corresponds to the first expression in Eq. (15). At this stage, both the component bodies and whole system are in the elastic

stage, the whole system is stable. The section ac corresponds to the second expression in Eq. (15). At this stage, the bearing capacity of the right body with low strength gradually decreases, while the bearing capacity of the left body with high strength still increases linearly and becomes the main bearing body gradually. The whole system is still stable due to the bearing capacity of the left body. The section cd corresponds to the third expression in Eq. (15). During this stage, the bearing capacity of the left body decreases gradually, and the whole system is stable before the left body becomes unstable. It can be seen that the high-strength component body determines whether the whole system is stable or not. By analyzing the section of the high-strength body of the third expression in Eq. (15) in the same way as that of double bodies with the same mechanical properties, the stable state of double bodies with different mechanical properties can be obtained. That is to say, applying Eqs. (12–14) to the strain softening stage of high-strength component body can determine the stable state of double bodies with different mechanical properties.

5 Conclusions

Single coal pillar–roof combined body and double coal pillar–roof combined bodies were designed to characterize single coal pillar–roof system and coal pillars–roof system in pillar goaf, respectively. A series of numerical simulations of uniaxial compression were conducted using PFC, the source inducement, failure modes and load transfer characteristics

of coal pillars–roof system were studied. On this basis, the instability criterions of double combined bodies with different combinations were deduced theoretically. Compared with existing researches, this study highlights four important conclusions:

- (1) Coal dominates the destruction during the single combined body is compressed. That is to say, coal is not only the first to be destroyed, but also induces rock damage. Meanwhile, the rock damage aggravates the destruction of coal in turn. Finally, the overall body loses bearing capacity based upon domino effect. The instability of a single coal pillar is the initial cause of the instability of the whole coal pillars–roof system in pillar goaf.
- (2) For double combined bodies with same mechanical properties, the two component bodies bear external load evenly and deform in coordination during compression. The whole system and its component bodies reach the bearing limits synchronously, and the loss of bearing capacity of any component body will lead to the instability of the whole system. When evaluating the stability of pillar goaf, the large-scale roof collapse disaster caused by the synchronous instability of coal pillars with the same or similar mechanical properties should be pay special attention to.
- (3) When double combined bodies with different mechanical properties are compressed, the low-strength body is damaged and reaches its bearing limit firstly. Concomitantly, the whole system reaches the first bearing peak as well. After that, as the external load originally borne by low-strength body transfers to the high -strength component body, the high-strength body reaches the bearing peak. Synchronously, the whole system reaches the second bearing peak. Thereafter, the high-strength body loses its stability gradually, resulting in the whole system no longer has bearing capacity simultaneously. For coal pillars with different mechanical properties in pillar goaf, it is necessary to accurately locate the coal pillars with weak bearing capacities and take reinforcement measures to prevent them from losing stability first, so as to prevent more coal pillars from losing stability due to load transfer.
- (4) The instability of any single component body can be regarded as the whole instability criterion of double bodies with same mechanical properties, while the instability of the single component body with high strength should be regarded as the instability criterion of the double bodies with different mechanical properties.

In the future, the failure and load transfer mechanism of multi coal pillar–roof combined bodies under more factors should be studied. Incidentally, the instability criterions should be applied to engineering pillar goaf to improve its practicability and accuracy.

Acknowledgements The authors would like to thank all editors and reviewers for patient comments and valuable suggestions of this paper.

Author contributions ZW and JL conceived and designed the study; LL and BL conducted the numerical simulations; LL and UI managed the data; BL and UI drew the figures; ZW and JL conducted the theoretical analysis; JL wrote the main manuscript text; all authors gave their final approval of the manuscript version to be submitted.

Funding This research was funded by the National Natural Science Foundation of Surface Project of China (Nos. 51774289 and 52074291).

Availability of data and materials The data that underlie the results of this manuscript and conclusions are presented in the figures and tables of this manuscript.

Declarations

Ethics approval and consent to participate Not applicable for studies not involving humans or animals.

Consent for publication The authors agree to publication in the journal indicated below and also to publication of the article in English by Springer's corresponding English-language journal.

Competing interests The authors declare that they have no known competing financial interests or personal relationships that could have appeared to influence the work reported in this paper.

Open Access This article is licensed under a Creative Commons Attribution 4.0 International License, which permits use, sharing, adaptation, distribution and reproduction in any medium or format, as long as you give appropriate credit to the original author(s) and the source, provide a link to the Creative Commons licence, and indicate if changes were made. The images or other third party material in this article are included in the article's Creative Commons licence, unless indicated otherwise in a credit line to the material. If material is not included in the article's Creative Commons licence and your intended use is not permitted by statutory regulation or exceeds the permitted use, you will need to obtain permission directly from the copyright holder. To view a copy of this licence, visit <http://creativecommons.org/licenses/by/4.0/>.

References

- Bai JW (2019) Research on the instability mechanism and prevention of residual coal pillars in the composite re-mining areas. *Taiyuan Univ Technol.* <https://doi.org/10.27352/d.cnki.gylgu.2019.000076>. (in Chinese)
- Bao XK, Guo JY, Liu Y, Zhao G, Cao JX, Wu JW, Zhao JC (2021) Damage characteristics and laws of micro-crack of underwater electric pulse fracturing coal-rock mass. *Theor Appl Fract Mech* 111:102853. <https://doi.org/10.1016/j.tafmec.2020.102853>
- Chen SJ, Xia ZG, Feng F, Yin DW (2020) Numerical study on strength and failure characteristics of rock samples with different hole defects. *Bull Eng Geol Environ* 80(2):1523–1540. <https://doi.org/10.1007/s10064-020-01964-y>
- Chen B, Shen B, Jiang H (2023) Shear behavior of intact granite under thermo-mechanical coupling and three-dimensional morphology of shear-formed fractures. *J Rock Mech Geotech Eng* 15(3):523–537. <https://doi.org/10.1016/j.jrmge.2022.04.006>
- Feng GR, Bai JW, Shi XD, Qi TY, Wang PF, Guo J, Wang SY, Kang LX (2021) Key pillar theory in the chain failure of residual coal pillars and its application prospect. *J China Coal Soc* 46(01):164–179. <https://doi.org/10.13225/j.cnki.jccs.2020.0927>. (in Chinese)
- Gao FQ, Kang HP, Yang L (2020) Experimental and numerical investigations on the failure processes and mechanisms of composite coal-rock specimens. *Sci Rep* 10(1):13422. <https://doi.org/10.1038/s41598-020-70411-5>
- Han PH, Zhang C, Wang W (2022) Failure analysis of coal pillars and gateroads in longwall faces under the mining-water invasion coupling effect. *Eng Fail Anal* 131:105912. <https://doi.org/10.1016/j.engfailanal.2021.105912>
- He YP, Huang QX, Wei YH, Du JW (2023) Research on roof load transfer by passing coal pillar of working face in shallow buried closely multiple-seam. *Minerals* 13(1):118. <https://doi.org/10.3390/min13010118>
- Huang BX, Liu JW (2013) The effect of loading rate on the behavior of samples composed of coal and rock. *Int J Rock Mech Min* 61:23–30. <https://doi.org/10.1016/j.ijrmms.2013.02.002>
- Li Z, Feng GR, Cui JQ (2020) Research on the influence of slurry filling on the stability of floor coal pillars during mining above the room-and-pillar Goaf: a case study. *Geofluids* 2020:8861348. <https://doi.org/10.1155/2020/8861348>
- Li T, Chen GB, Li QH, Cao B, Li YH (2022) The effect of crack characteristics on the mechanical properties and energy characteristics of coal-rock composite structure. *Acta Geodyn Geomater* 19(2):127–142. <https://doi.org/10.13168/AGG.2022.0003>
- Liu J, Wang EY, Song DZ, Wang SH, Niu Y (2015) Effect of rock strength on failure mode and mechanical behavior of composite samples. *Geomech Eng* 8(7):4527–4539. <https://doi.org/10.1007/s12517-014-1574-9>
- Liu XS, Tan YL, Ning JG, Lu YW, Gu QH (2018) Mechanical properties and damage constitutive model of coal in coal-rock combined body. *Int J Rock Mech Min* 110:140–150. <https://doi.org/10.1016/j.ijrmms.2018.07.020>
- Liu HF, Sun Q, Zhou N, Wu ZY (2021) Risk assessment and control strategy of residual coal pillar in room mining: case study in ecologically fragile mining areas, China. *Sustainability* 13(5):2712. <https://doi.org/10.3390/su13052712>
- Liu HT, Hao C, Wang ZW, Li C, Guo LF, Liang J, Wang HZ (2023) Study on stability of underlying room and pillar old goaf in close coal seam and mining of the upper coal seam. *Front Earth Sci* 10:1071250. <https://doi.org/10.3389/feart.2022.1071250>
- Ozturk H, Altinpinar M (2017) The estimation of uniaxial compressive strength conversion factor of trona and interbeds from point load tests and numerical modeling. *J Afr Earth Sci* 131:71–79. <https://doi.org/10.1016/j.jafrearsci.2017.04.015>
- Pan WD, Zhang SP, Liu Y (2020) Safe and efficient coal mining below the goaf: a case study. *Energies* 13(4):864. <https://doi.org/10.3390/en13040864>
- Poulsen BA, Adhikary D, Guo H (2018) Simulating mining-induced strata permeability changes. *Eng Geol* 237:208–216. <https://doi.org/10.1016/j.enggeo.2018.03.001>
- Prasetyo SH, Irnawan MA, Simangunsong GM, Wattimena RK, Arif I, Rai MA (2019) New coal pillar strength formulae considering the effect of interface friction. *Int J Rock Mech Min* 123:104102. <https://doi.org/10.1016/j.ijrmms.2019.104102>
- Qin SQ, Jiao JJ, Tang CA, Li ZG (2006) Instability leading to coal bumps and nonlinear evolutionary mechanisms for a coal-pillar-and-roof system. *Int J Solids Struct* 43(25–26):7407–7423. <https://doi.org/10.1016/j.ijsolstr.2005.06.087>
- Roos F, Bansal RC (2019) Reactive power and harmonic compensation: a case study for the coal-mining industry. *J Energy South Afr* 30(1):34–48. <https://doi.org/10.17159/2413-3051/2019/v30i1a2473>
- Sarfarazi V, Bahrami R, Bolbanabad SM, Matinpoor F (2023) Effect of the circle tunnel on induced force distribution around underground rectangular gallery using theoretical approach, experimental test and particle flow code simulation. *Struct Eng Mech* 84(5):633–649. <https://doi.org/10.12989/sem.2022.84.5.633>
- Song CH, Lu CP, Zhang XF, Wang C, Xie HD, Yan XY, Yang HW (2022) Moment tensor inversion and stress evolution of coal pillar failure mechanism. *Rock Mech Rock Eng* 55(4):2371–2383. <https://doi.org/10.1007/s00603-022-02783-1>
- Song C, Cao GM, Bai JW, Wang SY, Feng GR, Shi XD, Wang K, Zhu C (2023) Fracturing behaviors and mechanism of serial coal pillar specimens with different strength. *Materials* 16(7):2690. <https://doi.org/10.3390/ma16072690>
- Sun HT, Dai LC, Liu YB, Jin HW (2021) Critical conditions and energy transfer characteristics of the failure process of coal-rock combination systems in deep mines. *Geofluids* 2021:6655443. <https://doi.org/10.1155/2021/6655443>

- Tian Y, Gong PL, Zhao T, Yi K, Wen G (2023) Instability prediction model of remaining coal pillars under remaining disturbance. *Energy Sci Eng* 11(6):1842–1857. <https://doi.org/10.1002/ese3.1433>
- Yang J (2019) Experimental study on energy conversion law of coal and rock composite structure failure process. *Chongqing Univ.* <https://doi.org/10.1007/s12517-014-1574-9>. (in Chinese)
- Yang JX, Liu CY, Yu B, Wu FF (2015) The effect of a multi-gob, pier-type roof structure on coal pillar load-bearing capacity and stress distribution. *Bull Eng Geol Environ* 74(4):1267–1273. <https://doi.org/10.1007/s10064-014-0685-6>
- Yin DW, Chen SJ, Chen B, Xia ZG (2019) Simulation study on strength and failure characteristics of coal-rock composite sample with coal persistent joint. *Arch Min Sci* 64(3):609–623. <https://doi.org/10.24425/ams.2019.129372>
- Yin DW, Chen SJ, Ge Y, Liu R (2021) Mechanical properties of rock-coal bi-material samples with different lithologies under uniaxial loading. *J Mater Res Technol* 10:322–338. <https://doi.org/10.1016/j.jmrt.2020.12.010>
- Yu YJ, Liu JJ, Yang YT, Wang PB, Wang ZM, Song ZY, Liu JM, Zhao SQ (2022) Failure energy evolution of coal-rock combination with different inclinations. *Sci Rep* 12(1):19455. <https://doi.org/10.1038/s41598-022-23813-6>
- Zhang JX, Huang P, Zhang Q, Li M, Chen ZW (2017) Stability and control of room mining coal pillars-taking room mining coal pillars of solid backfill recovery as an example. *J Cent South Univ* 24(5):1121–1132. <https://doi.org/10.1007/s11771-017-3515-8>
- Zhao Z, Sun W, Chen S, Yin D, Liu H, Chen B (2021) Determination of critical criterion of tensile-shear failure in Brazilian disc based on theoretical analysis and meso-macro numerical simulation. *Comput Geotech* 134:104096. <https://doi.org/10.1016/j.compgeo.2021.104096>
- Zhou YJ, Li M, Xu XD, Li XT, Ma YD, Ma ZG (2018) Research on catastrophic pillar instability in room and pillar gypsum mining. *Sustainability* 10(10):3773. <https://doi.org/10.3390/su10103773>
- Zhou ZL, Wang HQ, Cai X, Zang HZ, Chen L, Liu F (2020) Bearing characteristics and fatigue damage mechanism of multi-pillar system subjected to different cyclic loads. *J Cent South Univ* 27(02):542–553. <https://doi.org/10.1007/s11771-020-4315-0>
- Zhou N, Du EB, Li M, Zhang JX, Dong CW (2021) Determination of the stability of residual pillars in a room-and-pillar mining goaf under eccentric load. *Energy Rep* 7:9122–9132. <https://doi.org/10.1016/j.egy.2021.11.140>
- Zhu WB, Chen L, Zhou ZL, Shen BT, Xu Y (2019) Failure propagation of pillars and roof in a room and pillar mine induced by longwall mining in the lower seam. *Rock Mech Rock Eng* 52(4):1193–1209. <https://doi.org/10.1007/s00603-018-1630-y>
- Zhukova AG, Mikhailova NN, Sazontova TG, Zhdanova NN, Kazitskaya AS, Bugaeva MS, Gorokhova LG, Arkhipenko YV (2020) Participation of free-radical processes in structural and metabolic disturbances in the lung tissues caused by exposure to coal-rock dust and their adaptogenic correction. *Bull Exp Biol Med* 168(4):439–443. <https://doi.org/10.1007/s10517-020-04727-7>

Publisher's Note Springer Nature remains neutral with regard to jurisdictional claims in published maps and institutional affiliations.